Progress In Electromagnetics Research, Vol. 141, 1–15, 2013

HIGH DEFINITION ELECTRICAL CAPACITANCE TOMOGRAPHY FOR PIPELINE INSPECTION

Marianthe Evangelidis, Lu Ma, and Manuchehr Soleimani*

Engineering Tomography Laboratory (ETL), Department of Electronic and Electrical Engineering, University of Bath, Bath, UK

Abstract—Pipelines made of dielectric materials such as Polyethylene (PE) are becoming increasingly popular. With no suitable inspection technique for dielectric pipes, there is an urgent need to develop new technology for their inspection. This paper presents a novel pipe inspection technique using Electrical Capacitance Tomography (ECT) imaging. Traditionally ECT is used for industrial process tomography as a low resolution but fast tomographic imaging technique. Typically commercial ECT can provide a resolution of approximately 10 percent of the imaging region. In this paper a limited region tomography technique is developed take into account prior knowledge about the geometry of the pipe. This has significantly enhanced the imaging resolution of the ECT system, making it a viable pipe inspection solution. The experimental results in this study demonstrate an interior wall loss area as small as 0.195 percent of the ECT cross sectional imaging region is repeatable and can be reliably detected. A narrowband pass filter method (NPFM) is used as a means to limit the region for the ECT algorithm. This results in an unprecedented resolution, making ECT a viable non-destructive evaluation (NDE) technique for plastic pipes. The NDE application of the ECT for PE pipes is demonstrated in this paper with several experimental results. A wall loss of depth of 1.5 mm could be detected for an ECT sensor array of 150 mm in diameter, showing a high resolution and high definition ECT (HD-ECT) imaging that has not been reported before.

Received 13 April 2013, Accepted 31 May 2013, Scheduled 7 July 2013

* Corresponding author: Manuchehr Soleimani (m.soleimani@bath.ac.uk).

1. INTRODUCTION

Plastic pipes are widely used in industry as they offer advantages in terms of cost, weight and easy installation. Pipelines have a variety of requirements involving safety and quality that need to be met. To ensure their compliance with these regulations inspection occurs during manufacture and subsequent operation of the pipes. Although there are several non-destructive evaluation (NDE) techniques developed for metallic pipes, there is not a reliable alternative for the inspection of plastic pipes. A defect that results in a leakage from a pipe can not only bring financial losses, but can also cause disastrous environmental and safety impacts. Ultrasonic and X-ray methods [1] are amongst the alternative non-invasive methods available for pipe inspection. X-ray radiography equipment is bulky, expensive and also requires special consideration for radiation protection. The ultrasonic method generally requires a contact medium and is not easily developed for different geometries. There is a great need for a robust method for the inspection of plastic pipes.

Electrical capacitance tomography (ECT) is a relatively mature imaging technique with wide range of applications in industrial process tomography [2]. Electrical capacitance data measured between pairs of electrodes are used to image the internal permittivity distribution. ECT is attractive as a non-invasive tomographic imaging technique. In the past two decades the development in the field has shown significant changes to the technology and its' relevant applications. Current industrial applications of ECT include pneumatic conveying, flame visualization [3–6], visualization of fluidized bed gas-solid two-phase concentration distribution [7], two-phase flow void fraction measurements and flow identification [8, 9]. There is still the provision for further development for a broader and more valuable span of practical usage. This paper presents a new application area for the ECT imaging as a novel inspection tool for plastic pipes.

ECT is an imaging technique that can measure the permittivity of objects non-invasively. With broad development perspectives, good safety performance and a faster processing procedure, this technique can potentially be an alternative to NDE techniques. Furthermore it is an economical choice due to its low cost of manufacture and computation. For ECT to have a chance of being used for NDE applications there has to be a large increase in imaging resolution. ECT suffers from low spatial resolution providing an image with resolution of around 10 percent of the imaging area. With this limited resolution ECT can not be used as an NDE device. However, the imaging resolution can be improved if prior assumptions are made

about the imaging medium and area of interest within the imaging region. In [10, 11], it was shown that volume cracks could be detected by using a level set method through simulations. In this paper, we have adopted a narrowband pass filtering method (NPFM) that was developed for metallic pipeline inspection using magnetic induction tomography (MIT) technique [12, 13]. A resolution of 2 percent of the area of imaging was reported in MIT for pipeline imaging. In this paper a resolution of less than 0.2 percent, 10 times better using the same method has been previously achieved in [12, 13]. The plastic pipeline inspection using MIT based on a NPFM was not studied, although MIT is sensitive to all three passive electromagnetic properties: conductivity, permittivity and permeability, only the reconstruction of conductivity and permeability were focused in [12, 13]. This paper is a follow up study that aims to investigate the capability of ECT as a pipeline inspection tool. The recent discovery in pipeline inspection using experimental ECT data is presented; the experimental results of internal defects on plastic pipelines are discussed. The aim of this work is to research and potentially expand the applications of ECT for material characterization, taking the inspection of plastic pipes as an example. This is the first time ECT has been used for an NDE application. Providing a resolution that can give vital information about the structure of the pipe.

2. ECT SYSTEM FOR PIPELINE IMAGING

The ECT system architecture used for pipeline inspection comprises of three main components; the capacitance sensor array, projection data acquisition system, and a host computer. The block diagram of our ECT system is shown in Figure 1.

The sensor ring consists of 12 electrodes mounted evenly on

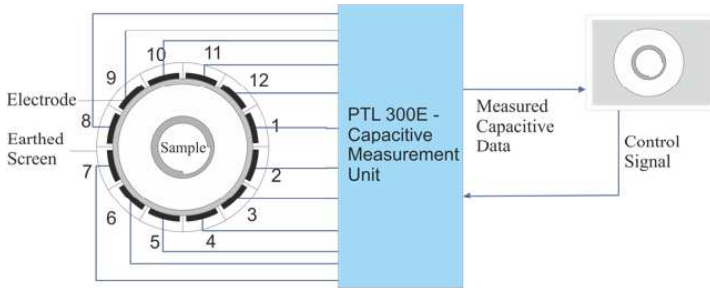

Figure 1. Block diagram of the ECT system architecture.

the external surface of a non-conducting perspex pipe [14]. An earthed screen surrounds the electrodes, this is primarily to protect the sensor system from the effects of any external electrical field changes. In similar systems a radial shielding between adjacent electrodes is usually employed, aiming to improve the sensor accuracy by reducing the standing capacitance and preventing the mutual influence between the adjacent electrodes. A commercial PTL300E-TP-G Capacitance Measurement Unit from Process Tomography Limited (http://www.tomography.com/) is used in our system for data collection. The unit uses a dual plane capacitance measurement unit of type DAM200E-TP-G. Sets of capacitance data can be collected at 100 frames per second for the 12-electrode sensor. The sensitivity of the measured data has an effective resolution of 0.1 fF and measurement noise level typically better than 0.07 fF. The ECT data is converted to a .txt file for measurement processing and image reconstruction in Matlab. A single plane of 12 electrodes with an imaging area of 150 mm in diameter is used for 2D ECT imaging in this study.

3. IMAGE RECONSTRUCTION

The ECT image reconstruction problem is an ill-posed inverse problem, to solve this inverse problem the forward problem needs to be solved [15–17]. In the ECT forward problem the excitation voltage and the permittivity distribution are given. Additional assumptions are made to calculate the interior electric field and electrode measurement values. Firstly the electrical conductivity, internal changes, magnetic field and the wave propagation effect are assumed to be negligible. The Poisson equation can then be used to construct the mathematical model of the forward problem in the terms of electric potential u

$$\nabla \cdot \varepsilon \nabla u = 0 \tag{1}$$

where ε is the dielectric permittivity in the inside region of the capacitance sensor shielding, excluding the electrodes and the radial shielding. The boundary conditions can be expressed as

$$u = V_k \tag{2}$$

for excitation electrodes with voltage V_k and

$$u = 0 \tag{3}$$

for the remaining (sensing) electrodes and shielding. The forward model calculates the capacitance value based on the given permittivity distribution. A finite element method was used for the forward problem [18]. As a result a mathematical model can be built and used for data analysis and computation in the inverse problem. For

a linear approach, the reconstruction is based on the assumption that the capacitance changes linearly with small changes in permittivity; this can be expressed using the Jacobian matrix [18]

$$J = \frac{dC}{d\boldsymbol{\varepsilon}} \tag{4}$$

where J is the Jacobian matrix; the derivative of measured capacitance C with respect to the permittivity. Many inversion algorithms were reported that could be used for ECT image reconstruction [16, 19–23]. In this study, the Newton one step error reconstruction (NOSER) algorithm is used to reconstruct the permittivity differences from the capacitance changes using the Jacobian matrix:

$$\Delta\varepsilon = (J'J + \alpha R)^{-1} J \cdot \Delta C \tag{5}$$

where R is diagonal matrix from $J'J$, and α is regularization parameter. For pipeline inspection a difference imaging mode is used where $\Delta C = C - C_r$, in which C_r is the reference capacitance data, and C is the measured capacitance for pipe under inspection. In this case $\Delta\varepsilon$ represents an image of permittivity differences from time difference capacitance measurements.

In [13], the authors present experimental results of metallic pipeline inspection using MIT, where the NPFM was shown capable of improving the limited resolution in MIT image reconstruction. In this study, we implemented NPFM in the ECT image reconstructions. The essence of implementing NPFM is to increase the accuracy by limiting the imaging area. Similar approaches have been reported in microwave and ultrasonic imaging [24, 25]. Several other inverse and imaging problems can potentially benefit from limited region tomography method proposed in this paper, including but not limited to [27–35]. In [25], a pre-processing method was used to apply a band-pass filtering to multiple-frequency data for microwave tomography. The proposed method enabled the efficient reconstruction of object in limited regions. A projected Landweber was used for the inversion algorithm. The NOSER algorithm used in this study is a suitable choice of algorithm. Figure 2 shows the narrowband region selected for pipeline imaging, this is selected to be larger than the actual pipe size so that it can tolerate a small displacement of the pipe centre from centre of imaging region.

In order to evaluate the imaging improvement offered by proposed NPFM a singular value decomposition (SVD) analysis of the Jacobian matrix is carried out. According to the Picard's criteria [26] the number of singular value above a given noise level represent the amount information that can be achieved from an ill-posed inverse problem. When comparing the inversion strategies, the number of

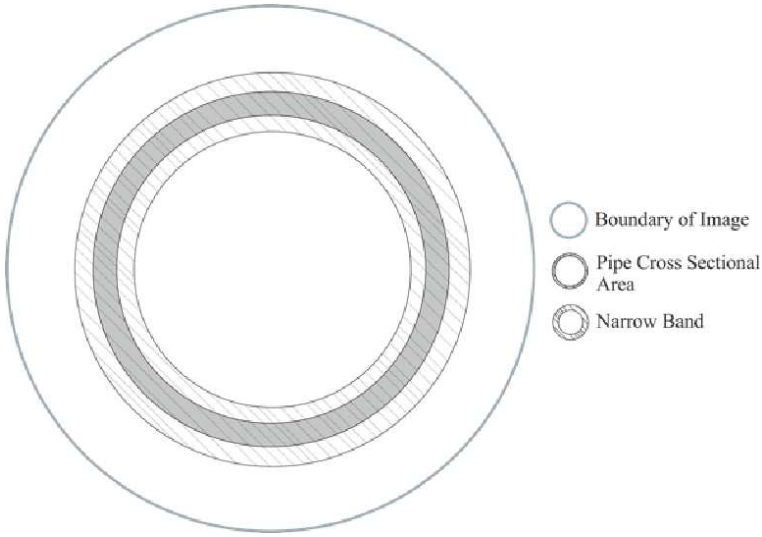

Figure 2. Narrow band region used for spatial filtering for limited region tomography.

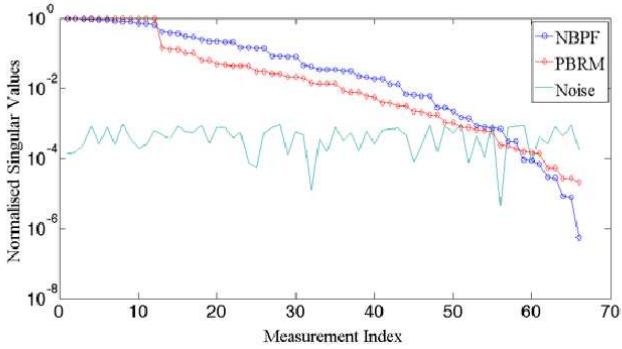

Figure 3. Singular value decay using both PBRM and NPFM. The red line represents the singular values obtained in the PBRM testing, the blue line shows the singular values from the NPFM testing.

unknowns also need to be considered. Figure 3 shows the singular value decay using the NPFM and the traditional pixel based reconstruction method (PBRM). In each case the singular value of the Jacobian matrix were calculated and normalized against the largest singular value of the same Jacobian. The normalization makes it possible to compare two image reconstruction strategies. The red line in Figure 3

represents the singular values obtained in the PBRM testing, while the blue line shows the singular values from the NPFM testing. As the assumed noise level is set to be 0.1 percent, the number of the singular values above the noise level is almost the same for both NPFM and PBRM. As the measured data remains unchanged for both cases, the improved resolution is due to the fewer number of unknown as a results of spacial filtering process. Moreover, due to the reduction in the number of pixels used in the reconstruction, the processing time is also reduced, which is an improvement of NPFM as computation time is an important factor in evaluating the quality of the reconstruction method. Another important improvement in NPFM is its robustness with regards to the regularization parameter α, a PBRM algorithm has a strong dependency on the selection of this parameter. In the better posed NPFM inverse problem the selection of this parameter in not critical. This is due the fact that the NPFM has an inherent regularization property due to spatial filtering effect. The narrowband region for a pipe with a circular cross-section in a circular sensor array has a relatively uniform sensitivity, which is better conditioned compared to PBRM where there are strong variations in sensitivity from a point very close to the sensor array to a point at the centre.

4. EXPERIMENTAL EVALUATION OF PIPELINE INSPECTION

4.1. Inspection of Pipes with Wall Removal

Three pipe samples are used for the inspection of pipes with wall removal. All three pipes are manufactured from polyethylene (PE), which has a relative permittivity of 2.25. The inner diameters of the pipes are 30 mm and the outer diameters of the pipes are 34 mm. The first column in Figure 4 shows a full pipe, a pipe with 1/6 wall removal, and a pipe with 1/4 wall removal. The images are reconstructed using both traditional PBRM and the NPFM, which are presented in the second and third columns respectively. We also include the post-processed images which show thresholding the reconstructed images from NPFM in Figure 4. With large wall removal both PBRM and NPFM will show the removed section. A clearer image can be seen when using NPFM. Although wall removal could be useful in leakage monitoring, alternative techniques can be used and it is not the objective for the NDE technique of a pipe. A histogram shape based method is used as a post-processing threshold to show the wall removal in the reconstructed images. In this case, the reference capacitance C_r is the free space capacitance data.

4.2. Inspection of Pipes with Interior Loss

It is of great interest to the NDE industry to be able inspect industrial pipes in terms of the interior loss of wall thickness. There are two pipe samples used in the following experiments; a small pipe sample with an external diameter of 88 mm and an internal diameter of 76 mm, and a larger pipe with an external diameter of 110 mm and an internal diameter 90 mm. The larger pipe is made from Polybutylene (PB), a thermoplastic with good mechanical properties and chemical resistance, and it is widely used for heating and plumbing applications in many properties. This PB pipe has an approximately relative permittivity of 2. The smaller pipe is manufactured from PE. The length of the small pipe and large pipe are 300 mm and 113 mm respectively. Three different samples are used. The dimensions are shown Figure 5, the images from left to right represent; one defect on the interior of the small pipe with a depth of 2.5 mm, 2 defects on the on the interior of the larger pipe and 1 defect of 1.5 mm depth on the interior of the small pipe. The dimensions of the defects are also shown. In the remaining experiments presented in this paper, the reference capacitance C_r is the data measured from a perfect pipe sample.

Figure 6 shows the experimental results of pipeline inspection with internal wall loss. The dimensions of the defects can be found

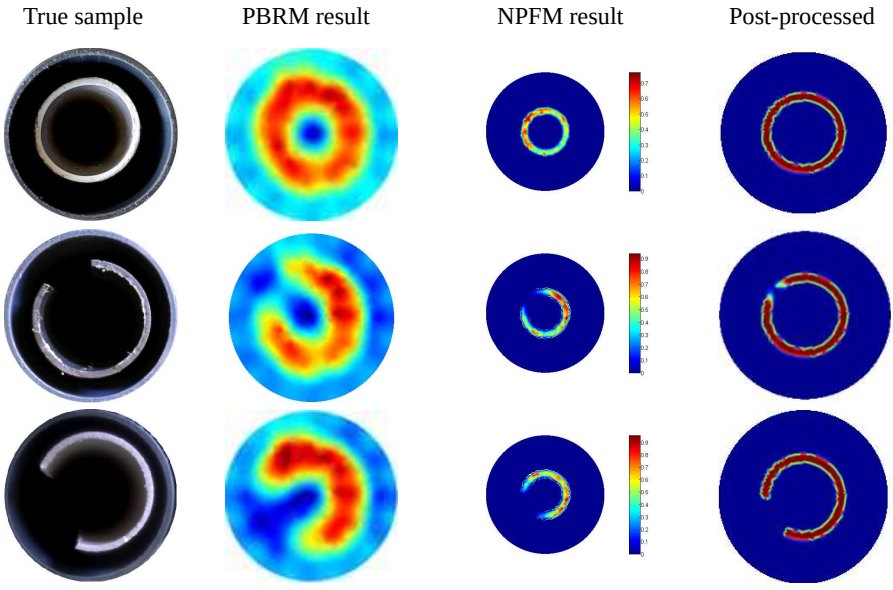

Figure 4. Inspection of pipelines with wall removal.

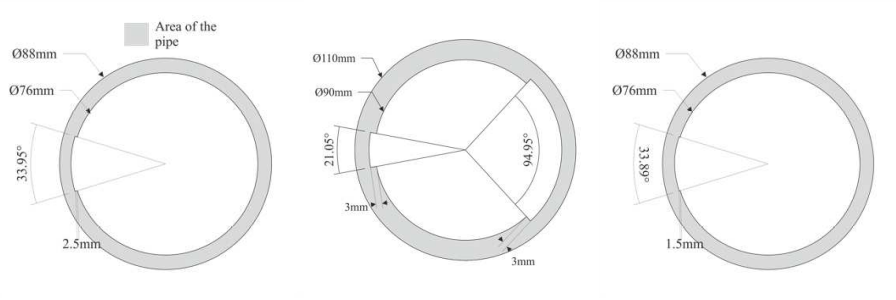

Figure 5. Pipes with defect(s) located on the interior. The schematic on the left contains defect of 25 mm in length along the interior circumference and 2.5 mm in depth, the 110 mm diameter pipe in the middle has 2 defects, one defect spans 50 mm on the interior circumference and the other 20 mm, located opposite one another both with a 3 mm depth. The 88 mm diameter pipe on the right hand side has a defect of 1.5 mm depth.

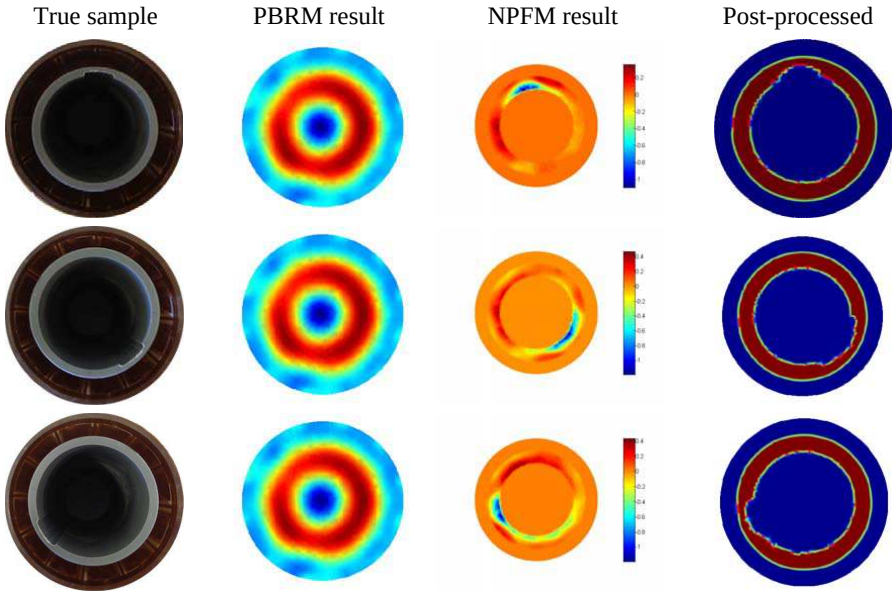

Figure 6. Pipe inspection with one interior defect of 2.5 mm, pipe has the same length as the ECT sensor. Defected pipes are shown in post-processed image.

in Figure 5. The use of the NPFM requires the pipes to be located in the centre of the sensor array. The position of the pipe becomes crucial, it was reported in [13] that this difficulty can be partially overcome by choosing a larger narrow band compared to the size of the pipe. All the measurements are compared to background readings, which are taken from a full pipe (without a defect) sample. The difference between the capacitance measurements of the defective pipe and perfect pipe are then found. The true samples, PBRM results, NPFM results and post-processed (with thresholding) images are shown in Figure 6. The same defect can be detected in various locations with respect to the sensor array. It can be seen that reconstructed images correspond clearly to the variation of the locations of the defects. The experimental results are repeatable and can be reliably detected in various placements.

The results comparing the pipe inspection using traditional PBRM and NPFM are shown in Figure 7. The sensor array has a diameter of 150 mm. In terms of the size of sensor the smallest measured defects when using a sample with two defects on was 0.29 percent of the cross sectional area of the imaging region.

It can be seen from Figure 8 that for a pipe with 12 mm thickness,

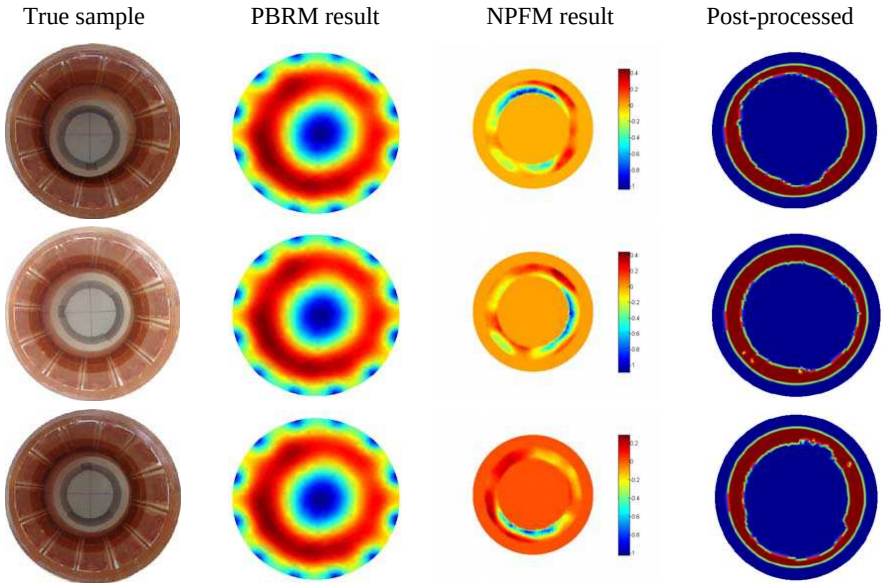

Figure 7. Pipe inspection with two interior defects, pipe is a half length of the ECT sensor. Defected pipes are shown in post-processed image.

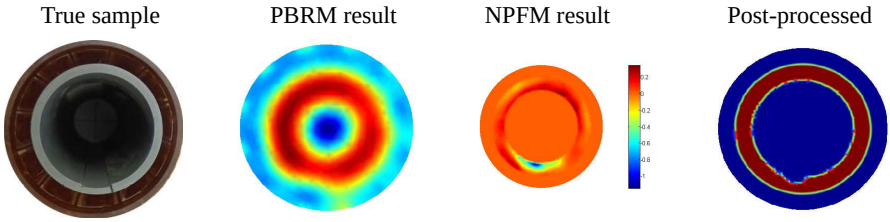

Figure 8. Smaller defect inspection with a defect of 1.5 mm, pipe has the same length as the ECT sensor. Defected pipes are shown in post-processed image.

a defect of 1.5 mm can be reliably detected, this has a spatial area resolution of 0.195 percent of the imaging region. The defect covers entire length of the sensor array (i.e., 2D ECT assumption) in results of Figures 4, 6, 8. In Figure 7, the defected pipe is only covers half of the length of the ECT sensor. In real life applications, a defect may include a smaller length in axial direction or have a non-uniform wall loss in axial direction. Three dimensional ECT is well established in past few years and may provide a suitable solution for such a situation, so that volume of defect can be analysed. Smallest defect volume that can be detected will then depend on accuracy of the ECT system and aspects of sensor design. If a 2D ECT system is used to image defect in a long pipeline system the time series information from defected images may enhance axial information. A combination of very small defects when they are placed close to each other will be seen as a single lareger defect. All these will be investigated in our future studies and are beyond scope of this paper.

In all these cases the PBRM could not give any useful information about the wall loss, and in all these cases the NPFM successfully locates the wall loss with the imaging defect size similar to the true wall loss. It is worth noticing that the ECT will be sensitive to fluid inside of the pipe, so the same results can not be achieved if an accurate assumption can not be made about the distribution of permittivity inside of the pipe under inspection. At this stage the proposed method can only be used when the pipe system is empty.

The high resolution ECT presented here is achieved through an inherent regularization and spatial filtering algorithm. It is obvious that high resolution imaging requires large number of image pixels. Large numbers of pixels in PBRM will have to be smoothed by a regularization term as the limited numbers of ECT measurement data can not recover all pixel values. A high resolution mesh can be used in NPFM by filtering out the unimportant parts of the ECT imaging

area. In this study a mesh of 12184 triangular elements was used for ECT imaging region 4122 in narrowband area. NPFM images shown with color bar, where negative image value represents defect part of the pipe.

5. CONCLUSION

In this paper a NPFM was developed for inspection of the plastic pipes using ECT imaging method. A wall loss covering only 0.195 percent of the ECT imaging area could be reliably detected. The resolution of 1.5 mm depth in a tomography array of 150 mm in diameter can be described as high definition ECT imaging. In this study 2D ECT method was adapted and the defect was created along the entire length of the pipe. The ECT is a fast imaging system that can potentially provide 100 images every second, this will make it a rapid NDE solution for plastic pipes. Proposed NPFM offers several advantages including reduced computational times for image reconstruction, robustness against the regularization parameter and an exceptionally good resolution for this application. Resolution achieved in this paper makes ECT a very promising and a viable solution for inspection of plastic pipes. The ECT is non-invasive and does not requires a contact medium make it potentially a more robust inspection method. The results demonstrated in this paper are very promising and encouraging. In our future work, more in-depth theory will be studied to improve the resolution. Furthermore, we aim to inspect the pipeline joints and cracks using ECT experimental data. A quantitative assessment of the imaging accuracy and the image quality will also be addressed, aiming to further develop the ECT technique as an automated NDE technology.

REFERENCES

1. Munns, I. J. and G. A. Georgiou, "Ultrasonic and radiographic NDT of butt fusion welded polyethylene pipes," *Insight*, Vol. 41, No. 5, 1999.
2. Sangworasil, M., Y. Kitjaidure, C. Yossontikul, and K. Chitsajul, "An electrical capacitance tomography," *Signal Processing 6th International Conference*, Vol. 2, 1766–1769, 2002.
3. Liu, S., Q. Chen, X. Xiong, Z. Zhang, and J. Lei, "Preliminary study on ect imaging of flames in porous media," *Measurement Science and Technology*, Vol. 19, No. 9, 094017, 2008.

4. Yang, W., "Design of electrical capacitance tomography sensors," *Measurement Science and Technology*, Vol. 21, 13, 2010.
5. Yan, Y., T. Qiu, G. Lu, M. Hossain, G. Gilabert, and S. Liu, "Recent advances in flame tomography," *Chinese Journal of Chemical Engineering*, Vol. 20, No. 2, 389–399, 2012.
6. Waterfal, R. C., R. He, P. Wolanski, and Z. Gut, "Flame visualizations using electrical capacitance tomography (ECT)," *Proc. SPIE 4188, Process Imaging for Automatic Control*, 242–250, 2001.
7. Fan, L. S., W. Warsito, and B. Du, "Electrical capacitance tomography imaging of gas-solid and gas-liquid-solid fluidized bed systems," *Journal of Visualization*, Vol. 7, No. 1, 2004.
8. Qiang, L. and Z. Yingna, "Review of techniques for the mass flow rate measurement of pneumatically conveyed solids," *Measurement*, Vol. 44, No. 4, 589–604, 2011.
9. Huang, Z., B. Wang, and H. Li, "Application of electrical capacitance tomography to the void fraction measurement of two-phase flow," *IEEE Transactions on Instrumentation and Measurement*, Vol. 52, No. 1, 7–12, 2003.
10. Soleimani, M., V. Stewart, and C. Budd, "Crack detection in dielectric objects using electrical capacitance tomography imaging," *Insight, Non-Destructive Testing and Condition Monitoring*, Vol. 53, No. 1, 21–24, 2011.
11. Hajihashemi, M. R. and M. El-Shenawee, "Inverse scattering of three-dimensional PEC objects using the level-set method," *Progress In Electromagnetics Research*, Vol. 116, 23–47, 2011.
12. Ma, L. and M. Soleimani, "Electromagnetic imaging for internal and external inspection of metallic pipes," *Insight, Non-Destructive Testing and Condition Monitoring*, Vol. 54, No. 9, 493–495, 2012.
13. Ma, L., H. Y. Wei, and M. Soleimani, "Pipeline inspection using magnetic induction tomography based on a narrowband pass filtering method," *Progress In Electromagnetics Research M*, Vol. 23, 65–78, 2012.
14. Peng, L., J. Ye, G. Lu, and W. Yang, "Evaluation of effect of number of electrodes in electrical capacitance tomography sensors on image quality," *IEEE Sensors Journal*, 1554–565, 2011.
15. Soleimani, M., C. N. Mitchell, R. Banasiak, R. Wajman, and A. Adler, "Four-dimensional electrical capacitance tomography imaging using experimental data," *Progress In Electromagnetics Research*, Vol. 90, 171–186, 2009.

16. Park, W.-K., "On the imaging of thin dielectric inclusions via topological derivative concept," *Progress In Electromagnetics Research*, Vol. 110, 237–252, 2010.
17. Banasiak, R., R. Wajman, D. Sankowski, and M. Soleimani, "Three-dimensional nonlinear inversion of electrical capacitance tomography data using a complete sensor model," *Progress In Electromagnetics Research*, Vol. 100, 219–234, 2010.
18. Soleimani, M., "Numerical modeling and analysis of the forward and inverse problems in electrical capacitance tomography," *International Journal of Information and System Sciences*, Vol. 1, No. 1, 193–207, 2005.
19. Wei, S. J., X. L. Zhang, J. Shi, and G. Xiang, "Sparse reconstruction for SAR imaging based on compressed sensing," *Progress In Electromagnetics Research*, Vol. 109, 63–81, 2010.
20. Jantan, A. B., R. S. A. Raja Abdullah, R. Mahmood, S. A. AlShehri, S. Khatun, and Z. Awang, "3D experimental detection and discrimination of malignant and benign breast tumor using NN-based UWB imaging system," *Progress In Electromagnetics Research*, Vol. 116, 221–237, 2011.
21. Ren, S., W. Chang, T. Jin, and Z. Wang, "Automated SAR reference image preparation for navigation," *Progress In Electromagnetics Research*, Vol. 121, 535–555, 2011.
22. Lei, J., S. Liu, Z. H. Li, and M. Sun, "Image reconstruction algorithm based on the extended regularized total least squares method for electrical capacitance tomography," *IET Sci. Meas. Technol.*, Vol. 2, No. 5, 326–336, 2008.
23. Zhao, J., J. Liu, Z. Li, W. Fu, and X. Li, "Image reconstruction algorithm based on updated sensitivity field for ECT," *Computer Engineering and Applications*, Vol. 48, No. 4, 2012.
24. Roberts, B. A. and A. C. Kak, "Reflection mode diffraction tomography," *Ultrasonic Imaging*, Vol. 7, No. 4, 300–320, 1985.
25. Salerno, E., "Microwave tomography of lossy objects from monostatic measurements," *IEEE Transactions on Microwave Theory and Techniques*, Vol. 47, No. 7, 986–994, 1999.
26. Hansen, P. C., "Rank-deficient and discrete ill-posed problems: Numerical aspects of linear inversion," *Society for Industria and Applied Mathematics*, Vol. 4, 1987.
27. Wei, H.-Y. and M. Soleimani, "Three-dimensional magnetic induction tomography imaging using a matrix free Krylov subspace inversion algorithm," *Progress In Electromagnetics Research*, Vol. 122, 29–45, 2012.

28. Wei, H.-Y. and M. Soleimani, "Two-phase low conductivity flow imaging using magnetic induction tomography," *Progress In Electromagnetics Research*, Vol. 131, 99–115, 2012.
29. Wei, H.-Y. and M. Soleimani, "Four dimensional reconstruction using magnetic induction tomography: Experimental study," *Progress In Electromagnetics Research*, Vol. 129, 17–32, 2012.
30. Cataldo, A., G. Cannazza, E. De Benedetto, and N. Giaquinto, "Experimental validation of a TDR-based system for measuring leak distances in buried metal pipes," *Progress In Electromagnetics Research*, Vol. 132, 71–90, 2012.
31. Xing, S., D. Dai, Y. Li, and X. Wang, "Arimetric SAR tomography using $L_{2,1}$ mixed norm sparse reconstruction method," *Progress In Electromagnetics Research*, Vol. 130, 105–130, 2012.
32. Wang, J., Z. Zhao, J. Song, X. Zhu, Z.-P. Nie, and Q. H. Liu, "Reconstruction of microwave absorption properties in heterogeneous tissue for microwave-induced thermo-acoustic tomography," *Progress In Electromagnetics Research*, Vol. 130, 225–240, 2012.
33. Kuznetsov, S. A., A. G. Paulish, A. V. Gelfand, P. A. Lazorskiy, and V. N. Fedorinin, "Matrix structure of metamaterial absorbers for multispectral terahertz imaging," *Progress In Electromagnetics Research*, Vol. 122, 93–103, 2012.
34. Liu, Z., Q. H. Liu, C.-H. Zhu, and J. Yang, "A fast inverse polynomial reconstruction method based on conformal fourier transformation," *Progress In Electromagnetics Research*, Vol. 122, 119–136, 2012.
35. Chen, J., J. Gao, Y. Zhu, W. Yang, and P. Wang, "A novel image formation algorithm for high-resolution wide-swath spaceborne SAR using compressed sensing on azimuth displacement phase center antenna," *Progress In Electromagnetics Research*, Vol. 125, 527–543, 2012.